

Computationally Efficient Concurrent Multiscale Framework for the Linear Analysis of Composite Structures

*Original*

Computationally Efficient Concurrent Multiscale Framework for the Linear Analysis of Composite Structures / Kaleel, I.; Petrolo, M.; Carrera, E.; Waas, A. M.. - In: AIAA JOURNAL. - ISSN 0001-1452. - STAMPA. - 57:9(2019), pp. 4019-4028. [10.2514/1.J057880]

*Availability:*

This version is available at: 11583/2751813 since: 2020-04-27T10:52:30Z

*Publisher:*

AIAA

*Published*

DOI:10.2514/1.J057880

*Terms of use:*

This article is made available under terms and conditions as specified in the corresponding bibliographic description in the repository

*Publisher copyright*

Nature --&gt; vedi Generico

[DA NON USARE] ex default\_article\_draft

(Article begins on next page)

# A computationally efficient concurrent multiscale framework for the linear analysis of composite structures

I. Kaleel<sup>\*</sup>, M. Petrolo<sup>†</sup> and E. Carrera<sup>‡</sup>  
*Politecnico di Torino, Torino, Italy, 10129*

A.M. Waas<sup>§</sup>  
*University of Michigan, 1320 Beal Avenue Ann Arbor, MI 48109-2140*

This paper presents a novel multiscale framework based on higher-order one-dimensional finite element models. The refined finite element models (FE) originate from the Carrera Unified Formulation (CUF), a novel and efficient methodology to develop higher-order structural theories hierarchically via a variable kinematic approach. The concurrent multiscale framework consists of a macroscale model to describe the structural level components interfaced with efficient CUF micromechanical models. Such micromechanical models can take into account the detailed architecture of the microstructure with high fidelity. The framework derives its efficiency from the capability of CUF models to detect accurate 3D-like stress fields at reduced computational costs. This paper also shows the ability of the framework to interface with different classes of representative volume elements (RVE) and the benefits of parallel implementations. The numerical cases focus on composite and sandwich structures and demonstrate the high-fidelity and feasibility of the proposed framework. The efficiency of the framework stems from comparisons with the analysis time and memory requirement against traditional multiscale implementations. The present paper is a companion of a linked work dealing with nonlinear material implementations.

## I. Nomenclature

$\mathbf{C}$	=	material coefficient matrix
$\bar{\mathbf{C}}$	=	homogenized material coefficient matrix
$\mathbf{D}$	=	differential operator matrix
$F_s$	=	expansion function of the variation
$F_\tau$	=	expansion function of the variable

---

<sup>\*</sup>Postdoctoral fellow, MUL<sup>2</sup> Group, Department of Mechanical and Aerospace Engineering, Corso Duca degli Abruzzi 24, 10129, Torino, Italy.

<sup>†</sup>Assistant Professor, MUL<sup>2</sup> Group, Department of Mechanical and Aerospace Engineering, Corso Duca degli Abruzzi 24, 10129, Torino, Italy.

<sup>‡</sup>Professor of Aerospace Structures and Aeroelasticity, MUL<sup>2</sup> Group, Department of Mechanical and Aerospace Engineering, Corso Duca degli Abruzzi 24, 10129, Torino, Italy.

<sup>§</sup>Richard A. Auhl Department Chair of Aerospace Engineering, University of Michigan, 1320 Beal Avenue Ann Arbor, MI 48109-2140

$E_1, E_2, E_3$	=	Young moduli
$G_{12}, G_{13}, G_{23}$	=	shear moduli
$l$	=	axial length
<b>K</b>	=	stiffness matrix
$N_j$	=	shape function of the variation
$N_i$	=	shape function of the variable
<b>p</b>	=	body force vector
<b>P</b>	=	point force vector
<b>q</b>	=	surface force vector
<b>r</b>	=	line force vector
<b>u</b>	=	displacement vector
$u_x, u_y, u_z$	=	displacement components
<b>V</b>	=	volume
<b>W</b>	=	work
$x, y, z$	=	reference system axes
$\delta$	=	virtual variation
$\epsilon$	=	strain vector
$\bar{\epsilon}$	=	homogenized strain vector
$\nu_{12}, \nu_{13}, \nu_{23}$	=	Poisson ratios
$\rho$	=	density
$\sigma$	=	stress vector
$\bar{\sigma}$	=	homogenized stress vector
$\Omega$	=	cross-section domain

## II. Acronyms

1D	=	One-dimensional
3D	=	Three-dimensional
CPU	=	Central Processing Unit
CUF	=	Carrera Unified Formulation
CW	=	Component-Wise
DOF	=	number of Degrees Of Freedom
FE	=	Finite Element

GB = Gigabyte  
GP = Gauss Point  
LE = Lagrange Expansion  
MB = Megabyte  
MPI = Message Parsing Interface  
PVD = Principle of Virtual Displacements  
RVE = Representative Volume Element

### III. Introduction

**A**DVANCED fiber-reinforced composite structures have extensively penetrated various components of aerospace structures, e.g., primary structures of aircraft and turbine blades. Currently, the design and certification of lightweight aircraft composite components depend extensively on experimental testing, which leads to budgetary and time constraints [1]. The exorbitant cost associated with design and testing of new composite structures can diminish by incorporating high-fidelity simulation tools [2]. Also, virtual testing frameworks can expand the design space at early stages and provide a possibility to consider configurations that were too complex to verify with purely empirical methods. Existing computational tools only account for a fragmented portion of the testing domain covering the various length and time scales with limited reliability and robustness. The microstructure can be very complex, e.g., 3D wovens or tens of fibers, and the direct numerical simulation unfeasible. Understanding physical behaviors such as failure at lower scales and bridging the effect accurately to upper scales can significantly boost the fidelity of simulations. An integrated multiscale structure and material modeling framework can account for complex interactions across multiple scales within the structural hierarchy of an aircraft component [3]. Even though tremendous advances in the field of computing has spearheaded the development of multiscale computational tools, improving the solution robustness and efficiency remains an active area of research with the aim to extend such methodologies to increasingly complex structures.

The macroscale constitutive modeling assumes the material point as a homogeneous and accounts for heterogeneities, such as inclusions and voids, through implicit mathematical formulations. Within a multiscale framework, the constitutive response at a material point interfaces with a lower scale with explicit heterogeneous definitions through homogenization [4]. Thus, the effective behavior originates through solving a micromechanical boundary value problem (BVP). In an FE framework, such an approach is often referred to as the  $FE^2$  scheme [5]. For example, Ladavèze et al. developed a LATIN based methods, which is a non-incremental iterative computational strategy for multiscale modeling [6] for the nonlinear modeling of composites. The  $FE^2$  scheme can tackle various classes of multiscale problems such as nonlinear analyses of composites [7], thermo-mechanical analyses of heterogenous solids [8], and the micro-diffusive

damage modeling with interface elements [9]. The fundamental disadvantage often associated with the FE<sup>2</sup> method is the computational cost, since every integration point in the macroscale has an associated micro BVP to be solved. In the case of nonlinear analyses, solutions require iterative strategies, thereby leading to an increased computational cost. The commonly adopted scheme to address the computational cost is the development of highly parallelized implementations [5, 10]. Fritzen et al. developed a massively parallel GPU implementation of a hybrid computational homogenization method for visco-plastic materials using the NVIDIA CUDA framework [11] to reach an overall speedup in the order of 10<sup>4</sup> with respect to high-performance FE implementations. Given that improving efficiency at lower scales can significantly boost the computational efficiency, the use of efficient analytical and semi-analytical methods at microscale is yet another commonly adopted approach [12, 13]. Lagoudas et al. developed a numerical scheme based on the Mori-Tanaka averaging scheme for elastoplastic predictions of binary composites [14]. The Generalized Method of Cells (GMC) originated a class of tools and extensions, such as the High-Fidelity Generalized Method of Cells (HFGMC), for the multiscale analysis of various kinds of hierarchical structures [4]. Within GMC, the unit cell has some sub-cells and the macroscopic constitutive equation couples with microscopic state variables. The HFGMC is a popular methodology to model damage and failure analysis at the constituent scales of composites [13, 15, 16]. Zhang et al. proposed a novel multiscale framework to predict the effective nonlinear response of composites coupling a macro FE model and an analytical micromechanical method based on the Concentric Cylinder Model (CCM) [17]. The framework can undertake the failure response analysis of hybrid 3D textile composites [18]. The method is computationally efficient because the subscale analysis is done analytically using a secant method and has been extended by Patel and Waas [19] to make the subscale model more accurate. Reduced multiscale methodologies based on reduced basis and proper orthogonal decomposition techniques are other successful techniques from literature [7, 20, 21]. These methods improve the computational efficiency of the framework by adopting model reduction for micro BVP. The RVE modeling requires only a few modes with significant decrements of the computational effort and negligible drops in accuracy. The objective of the present paper is to introduce a novel multiscale framework based on a class of refined FE. The refined FE stems from the CUF [22, 23]. The CUF is a method to generate higher-order 1D and 2D FE hierarchically. Over the course of last decades, CUF models have efficiently handled various classes of problems such as micromechanical progressive failure analysis of composites [24], rotordynamics [25], hygrothermal analysis [26] and incompressible flow analysis [27]. In this work, the ability of CUF models to provide accurate three-dimensional (3D) displacement and stress fields at a reduced computational cost leads to building an efficient multiscale framework. Analogous to standard FE<sup>2</sup> methods, the 1D CUF models the macroscale to describe the structural level components, e.g., open-hole specimens and coupons. Explicit FE computations at lower scales take place via the CUF-CW micromechanics tool, first introduced by Kaleel et al. in [28]. The vast spectrum of applicability of 1D CUF models enables to generate various classes of RVE architectures. The interfacing between the two scales uses homogenization techniques by exchanging stress, strain and material matrices. The computational effort augments further via the parallel implementation of the

proposed framework.

This paper is organized as follows: 1D CUF models are introduced in brief in Section IV together with the multiscale framework and the related parallel implementation. Three sets of numerical results for the multiscale analysis of various hierarchical structures are enlisted in Section V. Concluding remarks are outlined in Section VI.

#### IV. 1D CUF and multiscale framework

1D CUF models decomposes the 3D displacement field into an axial displacement function  $\mathbf{u}(y)$  and a cross-section expansion function  $F_\tau(x, z)$ . Therefore, the generalized displacement field,  $\mathbf{u}$  becomes

$$\mathbf{u} = \mathbf{u}_\tau(y)F_\tau(x, z), \tau = 1, \dots, M \quad (1)$$

where  $M$  is the number of terms in the expansion function  $F_\tau(x, z)$ . The choice of  $F_\tau$  and  $M$  remains arbitrary and defines the adopted structural theory and, for instance,  $F_\tau$  can use Taylor polynomials, trigonometric, harmonic or exponential expansions, and combinations thereof [22]. This work exploits Lagrange polynomials as expansion functions, henceforth referred to as LE models. The component-wise approach (CW), a modeling technique stemmed out of LE models, models both the macro and microscale components. CW employs nine-node (L9) Lagrange polynomial functions to describe the kinematic field over the cross-section of the beam element.

##### A. Finite element formulation

The displacement vector is

$$\mathbf{u}(x, y, z) = \{u_x \quad u_y \quad u_z\}^T \quad (2)$$

where  $u_x$ ,  $u_y$  and  $u_z$  are the components in the global coordinate system. The strain  $\epsilon$  and stress  $\sigma$  are

$$\epsilon = \{\epsilon_{xx} \quad \epsilon_{yy} \quad \epsilon_{zz} \quad \epsilon_{xy} \quad \epsilon_{xz} \quad \epsilon_{yz}\}^T, \quad \sigma = \{\sigma_{xx} \quad \sigma_{yy} \quad \sigma_{zz} \quad \sigma_{xy} \quad \sigma_{xz} \quad \sigma_{yz}\}^T \quad (3)$$

With small strain assumptions, the linear strain-displacement relations are

$$\epsilon = \mathbf{D}\mathbf{u} \quad (4)$$

where  $\mathbf{D}$  is the differential operator and its explicit expression is not reported here for the sake of brevity but can be found in [22]. The constitutive law is

$$\sigma = \mathbf{C}\epsilon \quad (5)$$

where  $\mathbf{C}$  is the material matrix [29]. The discretization along the beam axis adopts standard FE shape functions  $N_i(y)$  and the generalized displacement field becomes

$$\mathbf{u}(x, y, z) = F_\tau(x, z) N_i(y) \mathbf{u}_{\tau i}, \quad \tau = 1, \dots, M; \quad i = 1, \dots, p + 1 \quad (6)$$

where  $N_i$  is the beam shape function of order  $p$  and  $\mathbf{u}_{\tau i}$  is the nodal displacement vector,

$$\mathbf{u}_{\tau i} = \{u_{x\tau i} \ u_{y\tau i} \ u_{z\tau i}\}^T \quad (7)$$

The orders of expansion functions  $M$  and shape functions  $p$  remain independent. B2, B3 and B4 indicate two-, three- and four-node beam elements, respectively.

Governing equations make use of the Principle of Virtual Displacement (PVD),

$$\delta W_{int} = \delta W_{ext} \quad (8)$$

where  $W_{int}$  is the internal work done by the stresses,  $W_{ext}$  is the external work applied on the system and  $\delta$  denotes the virtual variation of the displacement. The virtual variation of the internal work is

$$\delta W_{int} = \int_l \int_\Omega \delta \boldsymbol{\epsilon}^T \boldsymbol{\sigma} \, d\Omega \, dl \quad (9)$$

where  $l$  and  $\Omega$  correspond to length of the beam and area of the cross-section, respectively. Further manipulation of Eq.9 using Eq. 4 and Eq. 5 leads to

$$\begin{aligned} \delta W_{int} &= \delta \mathbf{u}_{j s}^T \int_l \int_\Omega [N_j(y) F_s(x, z) \mathbf{D}^T \mathbf{C} \mathbf{D} F_\tau(x, z) N_i(y)] \, d\Omega \, dl \\ &= \delta \mathbf{u}_{j s}^T \mathbf{k}_{ij\tau s} \mathbf{u}_{i\tau} \end{aligned} \quad (10)$$

where  $\mathbf{k}_{\tau s i j}$  is the fundamental nucleus of the stiffness matrix of size  $3 \times 3$ . Indices  $i$  and  $j$  correspond to the beam shape functions  $N_i$  and  $N_j$ , respectively; while  $\tau$  and  $s$  to the cross-section expansion functions  $F_\tau$  and  $F_s$ , respectively. The explicit expressions of the nine components of the fundamental nucleus is not repeated here, but it is given in [22], with additional information on the implementation aspects. The virtual variation of the external work is

$$\begin{aligned} \delta W_{ext} &= \int_V \delta \mathbf{u}^T \mathbf{p} \, dV + \int_S \delta \mathbf{u}^T \mathbf{q} \, dS + \int_l \delta \mathbf{u}^T \mathbf{r} \, dl + \delta \mathbf{u}^T P_m \\ &= \delta \mathbf{u}^T \mathbf{f} \end{aligned} \quad (11)$$

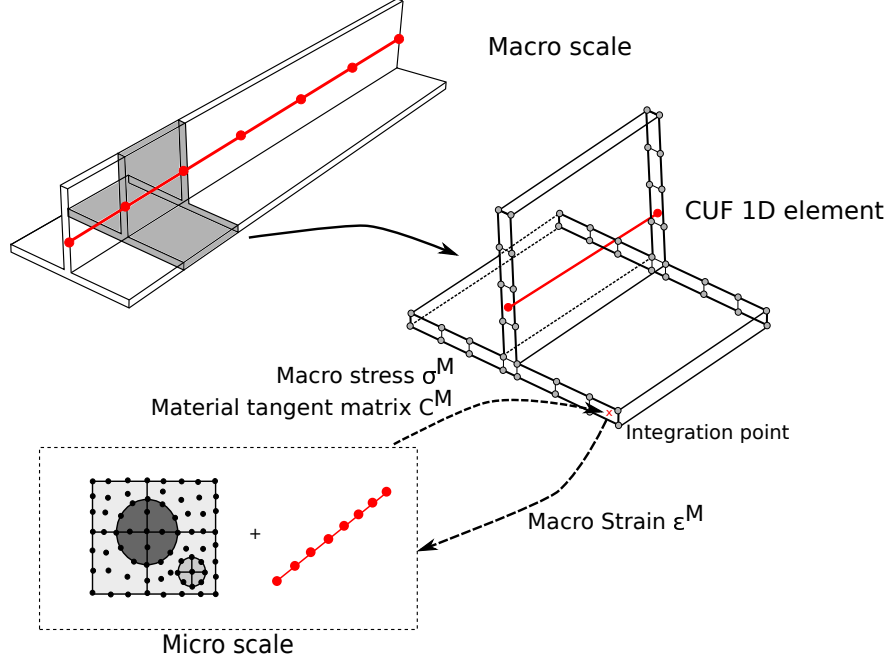


**Fig. 1 Illustration of multiscale modeling within the CUF framework**

where  $\mathbf{p}$ ,  $\mathbf{q}$ ,  $\mathbf{r}$  and  $P_m$  are body, surface, line and concentrated forces acting at point  $m$ , respectively. The equilibrium equation (Eq. 8) becomes

$$\delta \mathbf{u}_{js}^T \mathbf{k}_{ij\tau s} \mathbf{u}_{i\tau} = \delta \mathbf{u}_{js}^T \mathbf{f}_{js} \quad (12)$$

The assemblage of the global matrices and vector takes place as per classical FE schemes.

## B. Multiscale framework

The present multiscale framework makes use of the CUF micromechanics and macroscale modeling capabilities, as schematically illustrated in Fig. 1. In the proposed multiscale scheme, the material response of each integration point in the macro model originates from the application of macroscopic strain on micro RVE models through periodic boundary conditions. The scale transition between the scales makes use of homogenization, i.e., the volume averaging of the microscopic quantities in the microscale RVE.

## C. Micromodeling via the component-wise micromechanical framework

As in Fig. 2, the CUF micromechanics framework models the RVE as a beam structure using the CW approach [28]. The RVE model is 1D with the cross-section discretized in some Lagrange cross-sectional elements. The cross-section lays on the  $x_2 - x_3$  plane and extends along the beam direction, i.e., the  $x_1$  direction. The local refinement in the RVE stems from the discretization of the RVE using multiple L9 elements in the cross-section. The beam makes use of four-node cubic beam elements (B4). Periodic boundary conditions maintain the compatibility of displacements

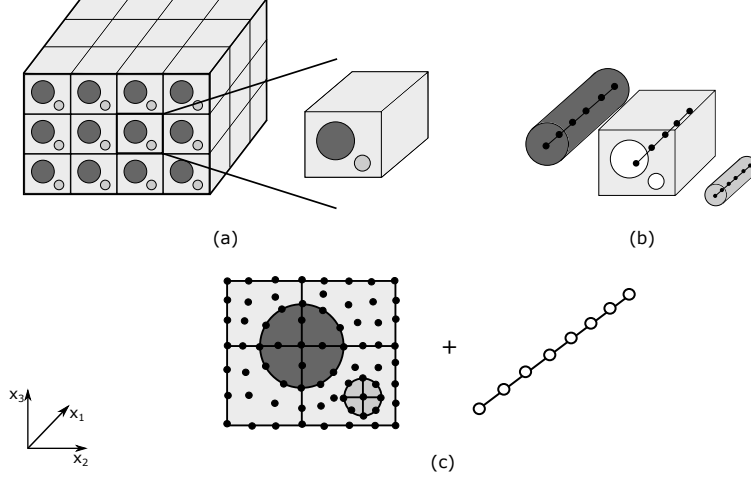


**Fig. 2** An illustration of a Component-Wise (CW) modeling of composite microstructure with arbitrary constituents: (a) a triply periodic composite microstructure with three different phases, (b) CW idealization of a triply periodic RVE with individual components modeled as separate components and (c) assembled cross-section with Lagrange elements along with the beams for the RVE [28]

and stress along the faces of the RVE. Readers are referred to the original paper by Kaleel et al. [28] on the CUF micromechanics framework for further information on the implementation. The homogenized response of the RVE is obtainable by volume averaging the stress and strain fields within all the constituents of the RVE,

$$\begin{aligned}\bar{\epsilon}_{ij} &= \frac{1}{V} \int_V \epsilon_{ij} dV \\ \bar{\sigma}_{ij} &= \frac{1}{V} \int_V \sigma_{ij} dV\end{aligned}\tag{13}$$

The overall stiffness matrix of the homogenized RVE becomes

$$\bar{\sigma}_{ij} = \bar{\mathbf{C}}_{ijkl} \bar{\epsilon}_{ij}\tag{14}$$

where  $\bar{\mathbf{C}}_{ijkl}$  is the homogenized stiffness of the RVE. The components  $\bar{\mathbf{C}}_{ijkl}$  matrix originate column-wise by computing the overall response based on applied individual unit strains.

#### D. Parallel implementation of multiscale framework

A standard single-scale FE implementation spends a significant amount of time on the stiffness matrix computation and global matrix decomposition for solution [30]. As the system grows large, the contribution from the latter tends to increase. In the case of multiscale frameworks, due to the requirement of solving significantly large sets of local problems associated with micro-solutions, the majority of the computational effort goes to the macro Gauss point update procedures. The proper handling of such a significant computational effort requires parallel implementations.

In this work, parallelization applies to the three most computationally intense tasks, namely, assembly of global matrices,

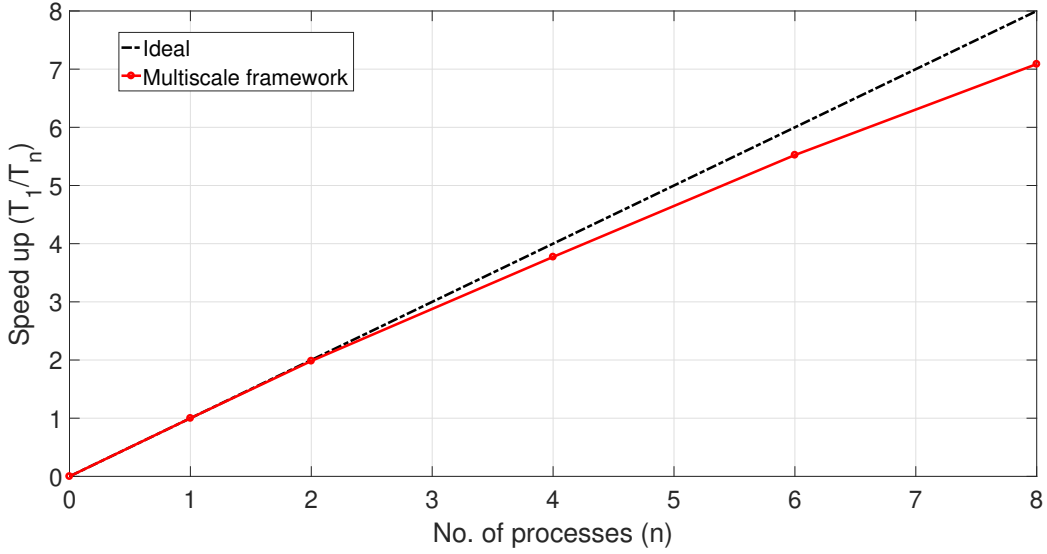


**Fig. 3** Speed-up obtained in the parallel version of multiscale framework for a system with  $\sim 130,000$  degrees of freedom

**Table 1** Nomenclature for various models used in multiscale analysis

Model name	Macroscale	Microscale
1D-1D	CUF beam element	CUF beam element
1D-3D	CUF beam element	Standard linear 3D brick element
3D-1D	Standard linear 3D brick element	CUF beam element

linear solution and macro Gauss point updates. The present framework makes use of standard MPI commands [31]. Finite elements distribute equally among various processors, and the corresponding stiffness matrix assembly is local and asynchronous. The computationally intensive macro integration point update procedure makes use of distributing macro integration points across various processes. Each process receives a set of Gauss points for generating macro solutions. Fig. 3 shows an example of the speed-up obtained using the parallel implementation un the proposed framework.

## V. Numerical results

This section deals with three sets of multiscale numerical examples. The first example predicts the stiffness of notched and unnotched specimens for various multidirectional laminate systems via square-packed RVE at the microscale. The second example presents the linear elastic analysis of an open-hole composite specimen under tension with a large randomly distributed fiber RVE. The last case deals with the analysis of a simply-supported honeycomb sandwich beam under bending load with a honeycomb core as RVE.

Table 1 shows the various multiscale modeling approaches adopted in this paper. The present framework handles both 1D and 3D models.

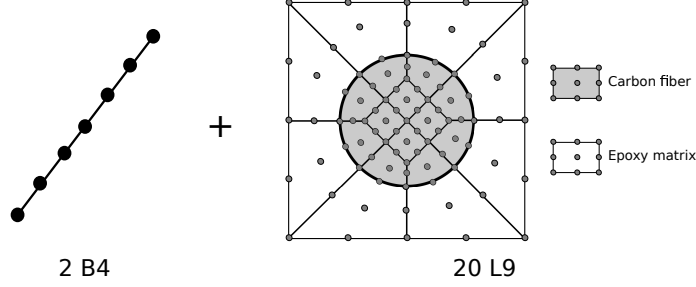


**Fig. 4 Microscale RVE model for stiffness prediction of multidirectional laminates**

**Table 2 Calibrated constituent properties of RVE for stiffness prediction of multidirectional laminates**

	$E_1$	$E_2$	$E_3$	$\nu_{12}$	$\nu_{23}$	$G_{12}$
	[GPa]	[GPa]	[GPa]	[-]	[-]	[GPa]
IM7 Fiber	256.0 <sup>T</sup> /215.0 <sup>C</sup>	15.0	15.0	0.28	0.19	15.0
Epoxy 977-3	3.2	3.2	3.2	0.38	0.38	1.16

T: Tension C: Compression

### A. Stiffness prediction of multidirectional laminates

This section presents results on the stiffness evaluation of three multidirectional laminates; namely, layup 1  $[0/45/90/-45]_{2s}$ , layup 2  $[60/0/-60]_{3s}$ , and layup 3  $[30/60/90/-30/-60]_{2s}$ . The numerical assessment focuses on the static tensile and compressive stiffnesses of notched and unnotched specimens made of IM7/977-3 graphite epoxy. Such structural configurations stem from the research work of Clay et al. on the state of the art of composite damage analysis [32, 33]. Dimensions  $304.8 \text{ mm} \times 38.1 \text{ mm}$  and the thickness of each layer is 0.125 mm, and the circular notch diameter is 6.35 mm. The prediction of the deformation and failure response of the aforementioned composite system is in Naghipour et al., via the NASA multiscale framework (FEAMAC) [16], and in Zhang et al. [34], via a two-scale computational model based on the smeared crack approach.

At the microscale, the geometry of the RVE is square-packed with a volume fraction of 65%, see Fig. 4. The calibration of the elastic material parameters of the RVE exploited the experimental results for uniaxial tension and compression tests [16, 32]. Table 2 summarizes the calibrated material properties of the individual constituents of the RVE. The square-packed RVE has 20 L9 and 2 B4 elements. Figure 5 shows the CW modeling of the macroscale unnotched and notched specimens. The notched specimen makes use of a three-component beam assembly. The far-notch beam - C2 - has a combination of B4 beam elements along with L9 cross-section elements and each C2 is 49 mm long. Whereas, the near-notch zone - C1 - uses a combination of B3 beam elements along with L9 elements. Table 3 enlists the details of the CUF models for each layup along with the computation time for the static analysis. The stiffness predictions for the unnotched and notched laminate systems are in Table. 4 along with comparisons against experimental and numerical results from the literature.

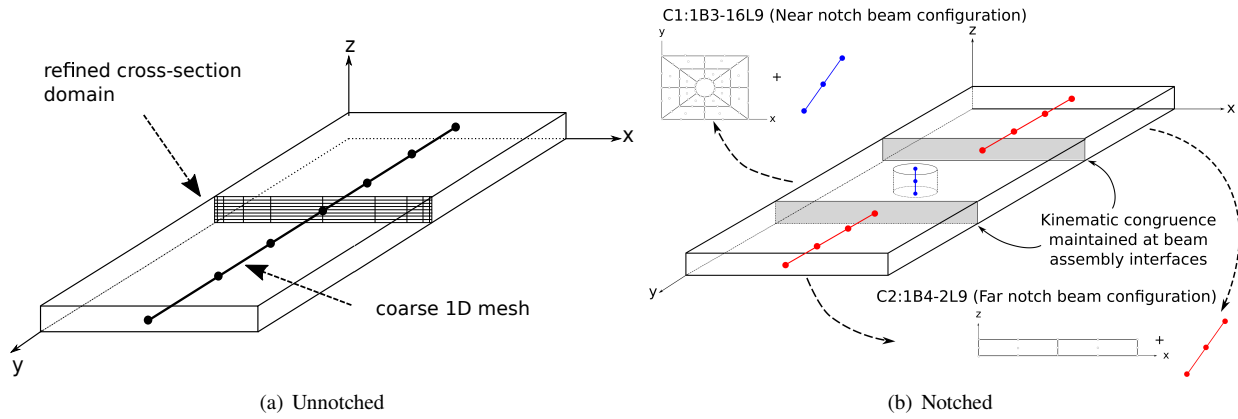


**Fig. 5** An illustration of the modeling of composite specimens using refined 1D CUF models for stiffness prediction of multidirectional laminates

**Table 3** Macro model information for stiffness prediction of multidirectional laminates

Model	Information	DOF	CPU Time (s)
<b>Layup 1:</b> $[0/45/90/-45]_{2s}$			
Unnotched	48 L9 - 4 B4	21,483	7.5
Notched	C2: 64 L9 - 4 B4 and C1: 80 L9 - 16 B3	45,540	19.1
<b>Layup 2:</b> $[60/0/-60]_{3s}$			
Unnotched	54 L9 - 10 B4	24,087	7.8
Notched	C2: 72 L9 - 4 B4 and C1: 80 L9 - 18 B3	48,708	20.3
<b>Layup 3:</b> $[30/60/90/-30/-60]_{2s}$			
Unnotched	60 L9 - 10 B4	26,691	8.9
Notched	C2: 80 L9 - 4 B4 and C1: 80 L9 - 20 B3	51,060	21.0

**Table 4 Stiffness prediction for notched and unnotched multidirectional laminates**

	Experimental [32]	MAC/GMC [16]	NCYL [34]	1D-1D
<b>Unnotched Tensile</b>				
Layup 1: [0/45/90/-45] <sub>2s</sub>	60.5	59.6 (1.49%)	60.6 (0.17%)	59.4 (1.82%)
Layup 2: [60/0/-60] <sub>3s</sub>	59.5	59.8 (0.50%)	61.5 (3.36%)	59.2 (0.50%)
Layup 3: [30/60/90/-30/-60] <sub>2s</sub>	38.0	39.0 (2.63%)	39.7 (4.47%)	39.1 (2.89%)
<b>Unnotched Compression</b>				
Layup 1: [0/45/90/-45] <sub>2s</sub>	48.0	51.0 (6.25%)	52.3 (8.96%)	50.9 (6.17%)
Layup 2: [60/0/-60] <sub>3s</sub>	48.9	51.2 (4.70%)	52.3 (6.95%)	51.0 (4.29%)
Layup 3: [30/60/90/-30/-60] <sub>2s</sub>	33.5	33.3(0.60%)	34.8 (3.88%)	34.11 (1.82%)
<b>Notched Tension</b>				
Layup 1: [0/45/90/-45] <sub>2s</sub>	48.3	49.1 (1.66%)	50.3 (4.14%)	49.4 (2.28%)
Layup 2: [60/0/-60] <sub>3s</sub>	48.8	48.9 (0.20%)	51.1 (4.71%)	50.44 (3.36%)
Layup 3: [30/60/90/-30/-60] <sub>2s</sub>	32.4	33.7 (4.01%)	34.5 (6.48%)	33.25 (2.62%)
<b>Notched Compression</b>				
Layup 1: [0/45/90/-45] <sub>2s</sub>	44.5	41.6 (6.52%)	41.9 (5.84%)	41.2 (7.42%)
Layup 2: [60/0/-60] <sub>3s</sub>	44.4	41.9 (5.63%)	41.9 (5.63%)	41.0 (7.70%)
Layup 3: [30/60/90/-30/-60] <sub>2s</sub>	30.1	29.2 (3.00%)	29.8 (1.00%)	28.63 (4.88%)

All units in GPa. Quantities in parenthesis represent error with respect to experimental results

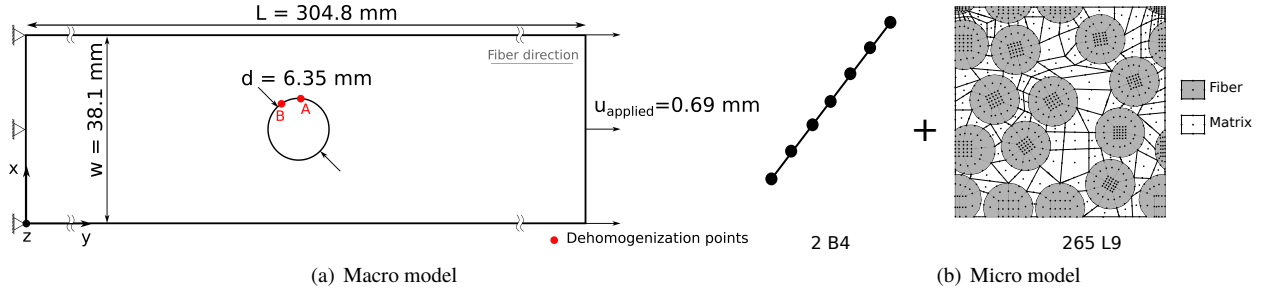


**Fig. 6 Geometry for linear multiscale simulation of a randomly distributed large RVE**

The numerical results suggest that

- 1) The present multiscale framework can predict the stiffness for a variety of multidirectional coupons with an accuracy level similar to the other numerical approaches from literature.
- 2) Considering experimental results, the error incurred by 1D-1D models for coupons under tension are below 4% whereas for coupons under compression is below 8%.
- 3) Although the present framework employs only 1D models, the results are accurate even for fairly complex configurations having discontinuities and non-prismatic elements.

### **B. Stress fields in a randomly distributed large RVE**

This section presents the capabilities of the present framework to compute efficiently local micro stress fields via a multiscale analysis. Based on the work of Ricks et al. [21], the numerical results focus on a notched rectangular specimen of dimensions 304.8 mm  $\times$  38.1 mm  $\times$  3.5 mm with a circular notch of diameter 6.35 mm, see Fig. 6(a). Fibers are parallel to the longitudinal axis of the specimen, and axial displacement of 0.69 mm is the applied boundary condition at one end of the specimen with the other end clamped. As in Fig. 5 (b), the open-hole specimen model adopts the CW technique with two sets of configurations, C2: 4 L9 - 2 B4 and C1: 80 L9 - 1 B3, for the far- and near-notch zones extending for 133.35 mm and 38.1 mm, respectively. The micro model is a randomly distributed fiber RVE as illustrated in Fig. 6 (b). The architecture of the RVE stems from Kaleel et al. [24, 28] and has 265 L9 with 2 B4 elements and the material properties are in Table 2. For comparison purposes, the numerical analysis uses a similar RVE model with 24,765 3D brick FE. The mesh configuration for the 3D FE micro model originated from a convergence study [28]. The present example exploits two classes of multiscale models, namely, 1D-1D and 1D-3D.

Figure 7 depicts the global von Mises stress distribution around the notch for 1D-1D and 1D-3D models. Local fields at locations A and B, see Fig. 6, around the notch are in Fig. 8 and Fig. 9, respectively. Table 5 presents the macro strain at the aforementioned macro Gauss point locations used for the dehomogenization. Numerical results enlisted in Table 6 provides information regarding the model size, analysis time and memory requirements. The analysis time focuses on two cases; one with computation and storage of local stress fields in micro RVEs, and the other one without it. Local

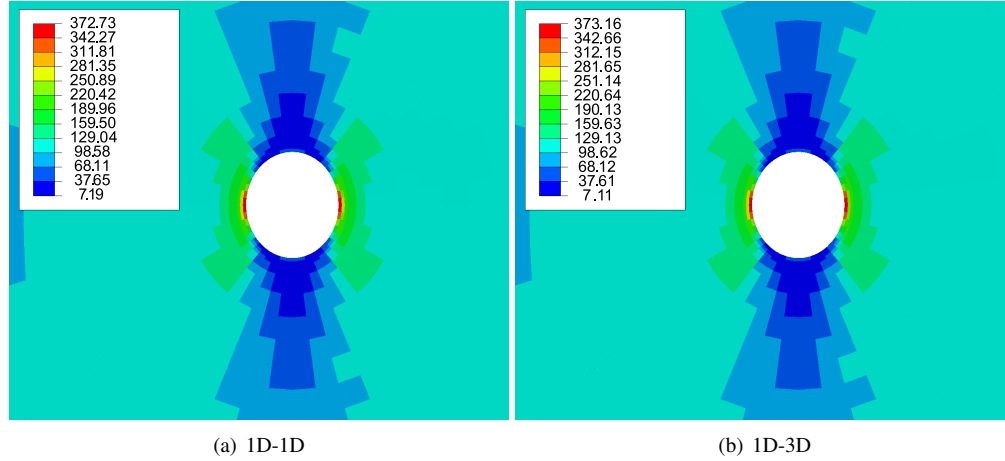


**Fig. 7** von Mises stress distribution around the hole for linear multiscale simulation of a randomly distributed large RVE

**Table 5** Dehomogenized strain computed at two locations for linear multiscale simulation of a randomly distributed large RVE

	$\epsilon_{22}$ $\times 10^{-3}$	$\epsilon_{11}$ $\times 10^{-3}$	$\epsilon_{33}$ $\times 10^{-3}$	$\epsilon_{23}$ $\times 10^{-4}$	$\epsilon_{13}$ $\times 10^{-4}$	$\epsilon_{12}$ $\times 10^{-3}$
<b>Location A (23.2, 152.4, 0.0)</b>						
1D-1D	-1.297	8.412	1.703	1.155	0.919	1.914
1D-3D	-1.309	8.478	-1.725	1.390	1.128	-1.936
<b>Location B (23.0, 151.9, 0.0)</b>						
1D-1D	1.011	3.553	-1.253	-3.136	-6.367	9.695
1D-3D	1.020	3.551	-1.261	-3.082	-7.771	9.745

stress fields in micro RVE requires the dehomogenization at every Gauss point in the macrostructure by passing on the global macro strain to respective micro RVE. Although, for the sake of brevity, the dehomogenized fields presented in this section concerns only points A and B. Memory required to store the local micro stress field is also computed.

Results suggest the following:

- 1) In comparison to 3D models at the microscale, 1D models can effectively capture the local fields with high accuracy.
- 2) Via the dehomogenization process and the refined local fields, the present modeling approach can detect highly local distributions of stress fields.
- 3) The results proved the capability of the multiscale framework to interface different kinds of higher-order FE at the microscale.
- 4) In comparison with the analysis time for 1D-3D, it is evident from Table 6 that 1D-1D requires only one-third of

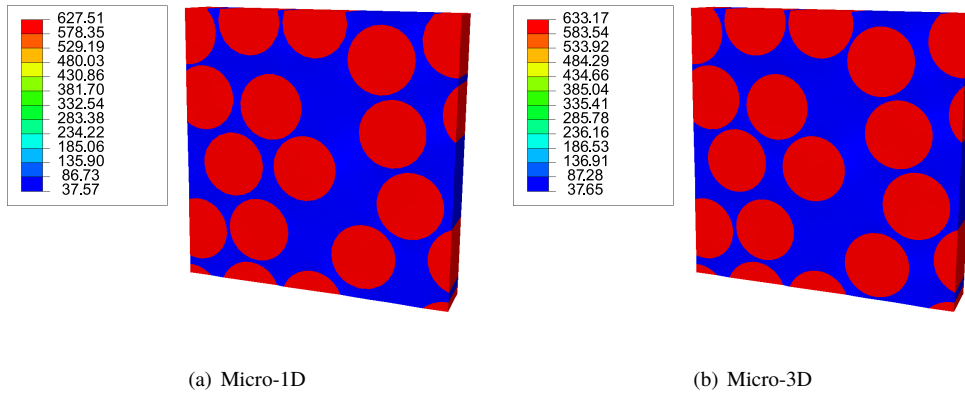


**Fig. 8** Local  $\sigma_{11}$  at point A for linear multiscale simulation of a randomly distributed large RVE

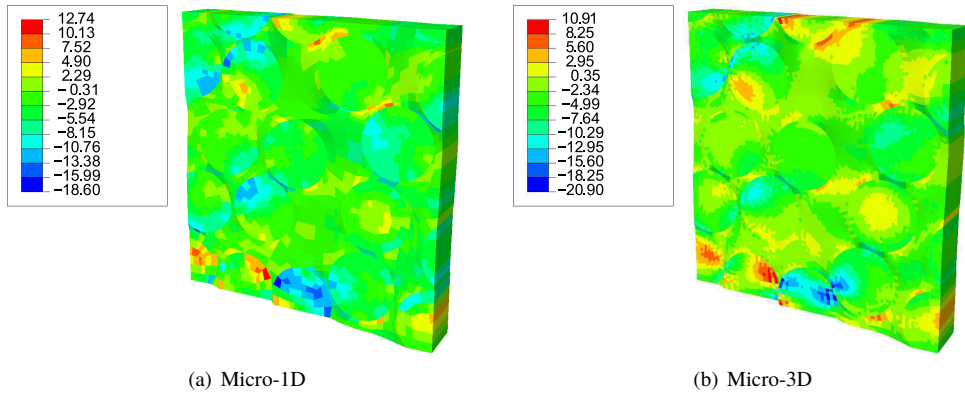


**Fig. 9** Local  $\sigma_{12}$  at point B for linear multiscale simulation of a randomly distributed large RVE

**Table 6** Numerical results for linear multiscale simulation of a randomly distributed large RVE

	Macro model		Micro model		Analysis time (s)		Memory required per macro GP <sup>1</sup> [MB]
	DOF	GP	DOF	GP	Without local micro fields	With local micro fields	
1D-1D	4,140	2,736	13,642	9,540	3.0	10.1	1.5
1D-3D	4,140	2,736	31,524	61,008	9.6	42.7	9.8

DOF: Degrees of freedom. GP: Gauss points.

<sup>1</sup> Required memory per each macro GP is calculated as 20 state variables stored per each Gauss point in the micro RVE using double precision real (8 bytes)

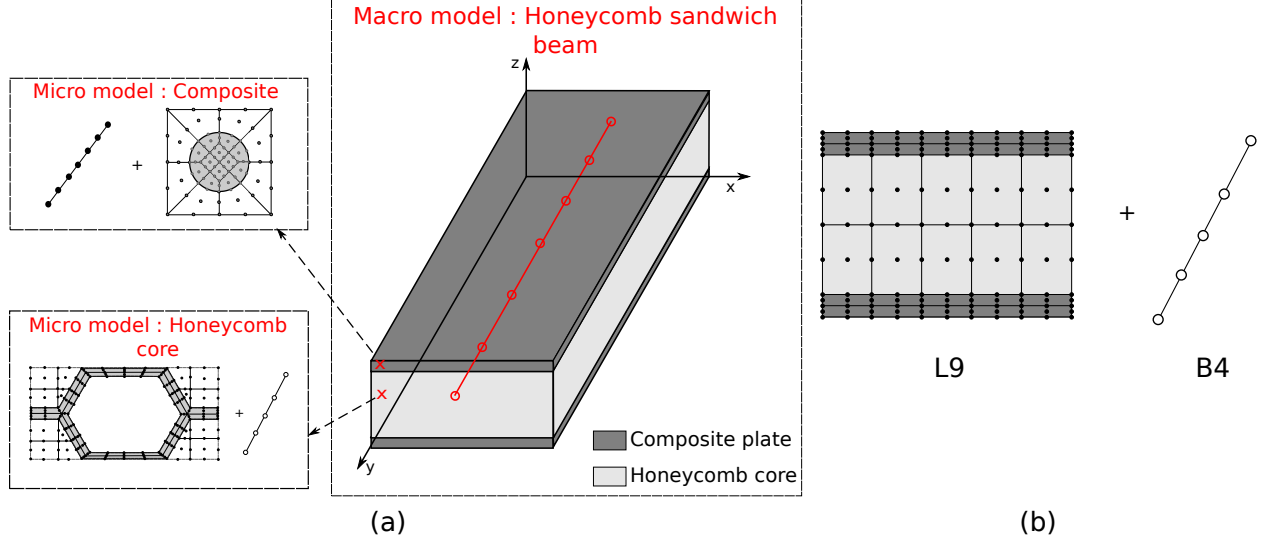


**Fig. 10 Multiscale modeling of honeycomb sandwich using CUF multiscale framework: (a) Interfacing two kinds of micro models for sandwich beam and (b) Component-Wise discretization of macro sandwich beam model using L9 cross-section and B4 beam elements**

**Table 7 Geometrical properties of core for multiscale structural analysis of honeycomb sandwich beam [35]**

$l_1$ (mm)	$l_2$ (mm)	$t_c$ (mm)	$\theta$ (deg)	$h_c$ (mm)
3.66	1.833	0.0635	60	20

the time for analyses without local fields and one-fourth of the time for analyses with local fields.

- 5) The efficiency of 1D-1D concerns also the memory requirements for the two models. In fact, 1D-1D led to a 6.5 times savings regarding the total memory required to store the local fields.

### C. Simply-supported honeycomb sandwich beam under bending loading

The current numerical example highlights the capabilities of the CUF multiscale framework to handle multiple types of RVE efficiently as in a honeycomb sandwich beam. The numerical example consists of a simply-supported honeycomb sandwich structure with an aluminum core and composite face sheets under bending loading, see Fig. 10. The face sheet consists of a laminate  $[0]_2$  modeled through the RVE described in the previous example (Section V.A). Based on the work of Catapano and Montemurro [35], the honeycomb properties are in Table 7 and Fig. 11. The honeycomb core is of aluminum with Young modulus  $E$  of 70 GPa and Poisson ratio  $\nu$  of 0.33 and density  $\rho$  of  $2.7 \times 10^{-6} \text{ kg/mm}^3$ . As discussed in the original paper on CUF micromechanics [28], additional void elements, i.e., elastic air, maintain the RVE consistent with the micromechanical homogenization formulation. As depicted in Fig. 12, the RVE has 286 L9 elements and 2 B4 elements amounting to a total degrees of freedom of 25,389. Table 8 enlists the predicted elastic properties of the honeycomb with comparison against results from the literature.

The macro model is a simply-supported sandwich honeycomb beam of length 700mm. As in Fig. 13, a uniform

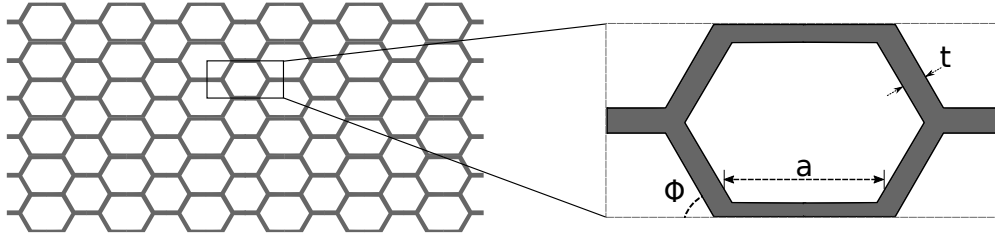


Fig. 11 Geometry of the honeycomb core: (a) Repeating core structure and (b) geometrical parameters of RVE

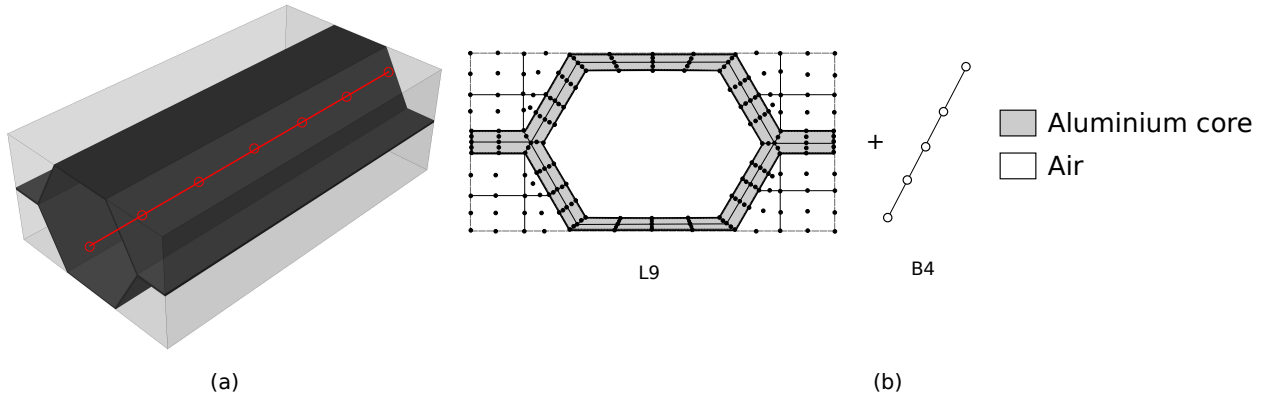
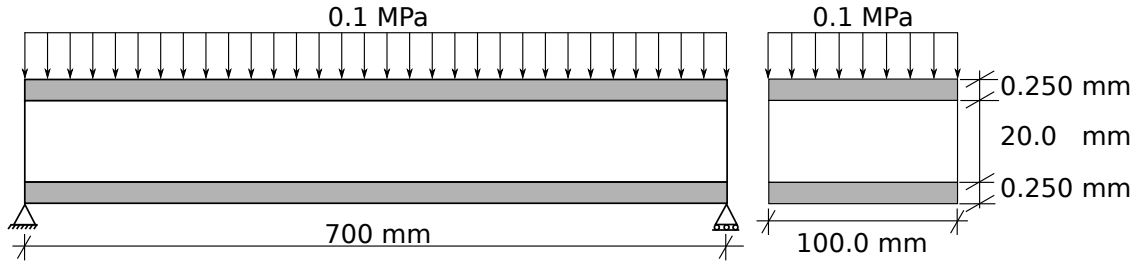


Fig. 12 Component-Wise modeling of the honeycomb core RVE, (a) CUF beam model of RVE and (b) cross-section and beam discretization

Table 8 Prediction of effective properties of honeycomb RVE for multiscale structural analysis of honeycomb sandwich beam

	CUF-Micro	MSG2D [36]	Catapano et al. [35]	Burton et al. [37]	Grediac [38]
$E_1$ (MPa)	0.935	0.884	0.884	0.815	0.815
$E_2$ (MPa)	0.969	0.918	0.918	0.815	0.815
$E_3$ (MPa)	1814.8	1812.3	1812.3	1848.2	1848.2
$G_{12}$ (MPa)	0.591	0.565	0.640	0.489	0.489
$G_{23}$ (MPa)	263.8	262.6	262.9	260.6	260.6
$G_{13}$ (MPa)	386.4	384.5	390.8	156.3 (LB) 434.3 (UB)	397.1
$\nu_{12}$ (-)	0.98	0.98	0.98	1.00	1.00
$\nu_{23}$ (-)	$1.70 \times 10^{-4}$	$1.67 \times 10^{-4}$	$1.61 \times 10^{-4}$	$1.45 \times 10^{-4}$	$1.45 \times 10^{-4}$
$\nu_{13}$ (-)	$1.76 \times 10^{-4}$	$1.61 \times 10^{-4}$	$1.67 \times 10^{-4}$	$1.45 \times 10^{-4}$	$1.45 \times 10^{-4}$
$\rho$ (kgmm <sup>-3</sup> )	$7.02 \times 10^{-8}$	$6.99 \times 10^{-8}$	$6.99 \times 10^{-8}$	$7.12 \times 10^{-8}$	-

LB: Lower bound, UB: Upper bound



**Fig. 13 Geometry and boundary conditions for multiscale modeling of honeycomb sandwich using CUF multiscale framework**

**Table 9 Macro model information for analysis of honeycomb sandwich beam**

Model	Information	DOF	GP
1D-1D	CUF beam element (36 L9 - 15 B4)- 1 L9 per layer for composite and 2 L9 per layer for core	19,734	16,200
3D-1D (Coarse)	12500 standard 3D brick element <sup>1</sup> - Mesh seed along the beam : 50 - One brick element per layer for composite and 4 brick element for core	43,758	100,000
3D-1D (Refined)	20000 standard brick element <sup>1</sup> - Mesh seed along the beam: 80 - One brick element per layer for composite and 4 brick element for core	69,498	160,000

DOF: Degrees of freedom. GP: Number of Gauss points. <sup>1</sup> Full integration (8 Gauss points per element)

pressure of 0.01 MPa acts on the top surface of the beam. As discussed previously, Gauss points belonging to the composite face sheet interface with fiber-reinforced micro CUF RVE models having 20 L9 and 2 B4 elements, see Fig. 4. The honeycomb aluminum core Gauss points act along the honeycomb core RVE micro model. Table 9 enlists the three classes of multiscale models used for the example. Table 10 shows the details concerning micro models.

Table 11 presents the numerical results including maximum displacements and the von Mises stress  $\sigma_{vm}$  at mid-span, analysis time, memory requirements for the total storage of microstate solutions, and the comparison between analysis time with and without local micro fields. Figure 14 shows the local von Mises stress field at (50.0, 35.0, 16.9) in the core of the sandwich honeycomb beam.

The numerical results suggest that

- 1) The present framework can deal with multiple 1D micro models interfaced with macro 1D models and 3D brick models.
- 2) From Table 11, 1D-1D models utilizes 1 CPU to obtain the results with and without local micro fields in 14.9 s

**Table 10 Macro model information for analysis of honeycomb sandwich beam**

RVE Model	Information	DOF	GP
Composite face sheet	CUF beam element (20 L9 - 2 B4)	1,869	1,440
Honeycomb core	CUF beam element (120 L9 - 2 B4)	25,389	20,596

**Table 11 Numerical results for analysis of honeycomb sandwich beam under bending load**

Model	Number of CPUs	Macro model		Analysis time (s)		Memory required for all macro GPs [GB] <sup>1</sup>
		Max disp (mm)	Max $\sigma_{vm}$ (MPa)	without local fields	with local fields	
1D-1D	1	4.61	121.7	14.9	64.0	2.95
3D-1D (Coarse)	4	4.50	118.8	27.9	181.2	19.8
3D-1D (Refined)	4	4.56	120.5	44.0	287.0	31.6

DOF: Degrees of freedom. GP: Gauss point.

<sup>1</sup> Required memory for all macro GP is calculated as 10 state variables (double precision real - 8 bytes) stored per each Gauss point in the micro RVE multiplied by total number of macro GP. Micro Gauss points for elastic air in micro core RVE is not included.

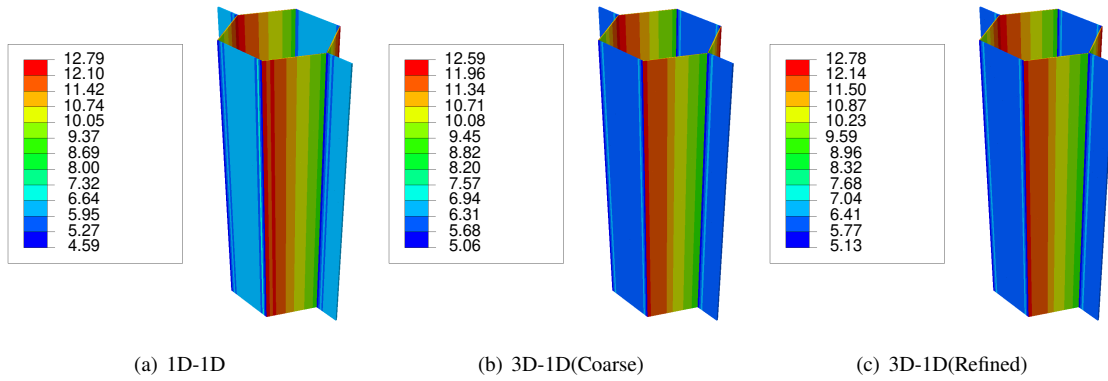


**Fig. 14 Local von Mises stress field  $\sigma_{vm}$  obtained at a point in core (50.0, 35.0, 16.9) for analysis of honeycomb sandwich beam for different multiscale models**

and 64.0 s, respectively. Whereas, the analysis time for 3D-1D (refined) with and without micro fields is 44.0 s and 287.0 s, respectively, via 4 CPUs. The stark difference stems from the fact that macro 3D requires a higher number of Gauss points, which in turn increases the time required for the analysis drastically.

- 3) Table 9 shows that the 1D macro model required 16,200 Gauss points but 3D macro models required 100,000 and 160,000 for coarse and refined configurations, respectively. The difference in required Gauss point translates to large variation in the memory required to store microstate solutions at all macro Gauss points. 1D-1D models require only 2.95 GB to store all the micro solutions whereas coarse and refined configurations of 3D-1D models require 19.8 GB and 31.6 GB, respectively, see Table 11.
- 4) Dehomogenization of the core at a given point by different multiscale models exhibits similar von Mises stress fields as shown in Fig. 14.

## VI. Conclusions

The paper presented a computationally efficient concurrent multiscale framework for modeling composite structures. The proposed framework adopts the CUF to generate a series of structural theories through variable kinematic descriptions. Via concurrent multiscale modeling, interfacing involves the CUF macroscale for structural level components and the CUF micromechanical approach. The latter can model different classes of RVE with various architectures and material compositions with a reduced computational cost with significant reductions of the overall computational overhead of the multiscale analysis. The numerical results show that

- 1) Multifold improvements concerning the analysis time and memory usage are achievable.
- 2) Via dehomogenization, the presented framework can predict very accurate local effects and 3D stress fields.
- 3) There are no restrictions on the complexity of the microstructure or of the number of coexisting microstructures.

This paper is linked to a work focusing on the material nonlinear capabilities of the framework.

## VII. Acknowledgment

This research work is part of the project FULLCOMP (FULLY analysis, design, manufacturing, and health monitoring of COMPOSITE structures), funded by the European Union Horizon 2020 Research and Innovation program under the Marie Skłodowska-Curie grant agreement No. 642121. Authors would also like to acknowledge the computational resources provided by HPC@POLITO (<http://hpc.polito.it>).

## References

- [1] Falzon, B. G., and Tan, W., “Virtual Testing of Composite Structures: Progress and Challenges in Predicting Damage, Residual Strength and Crashworthiness,” *The structural integrity of carbon fiber composites*, Springer, 2017, pp. 699–743. doi:10.1007/978-3-319-46120-5\_24.

- [2] Yang, Q. D., Cox, B. N., Fang, X. J., and Zhou, Z. Q., “Virtual testing for advanced aerospace composites: advances and future needs,” *Journal of Engineering Materials and Technology*, Vol. 133, No. 1, 2011, p. 011002. doi:10.1115/1.4002637.
- [3] Liu, X., Furrer, D., Kusters, J., and Holmes, J., “Vision 2040: A Roadmap for Integrated, Multiscale Modeling and Simulation of Materials and Systems,” NASA Glenn Research Center, 2018.
- [4] Aboudi, J., Arnold, S. M., and Bednarczyk, B. A., *Micromechanics of Composite Materials*, Butterworth-Heinemann, Oxford, 2013. doi:10.1016/C2011-0-05224-9.
- [5] Feyel, F., and Chaboche, J. L., “FE2 multiscale approach for modelling the elastoviscoplastic behaviour of long fibre SiC/Ti composite materials,” *Computer Methods in Applied Mechanics and Engineering*, Vol. 183, No. 3, 2000, pp. 309 – 330. doi:[https://doi.org/10.1016/S0045-7825\(99\)00224-8](https://doi.org/10.1016/S0045-7825(99)00224-8), URL <http://www.sciencedirect.com/science/article/pii/S0045782599002248>.
- [6] Ladevèze, P., Loiseau, O., and Dureisseix, D., “A micro–macro and parallel computational strategy for highly heterogeneous structures,” *International Journal for Numerical Methods in Engineering*, Vol. 52, No. 1-2, 2001, pp. 121–138. doi:10.1002/nme.274.
- [7] Radermacher, A., Bednarczyk, B. A., Stier, B., Simon, J., Zhou, L., and Reese, S., “Displacement-based multiscale modeling of fiber-reinforced composites by means of proper orthogonal decomposition,” *Advanced Modeling and Simulation in Engineering Sciences*, Vol. 3, No. 29, 2016, pp. 1–23. doi:10.1186/s40323-016-0082-8.
- [8] Özdemir, I., Brekelmans, W., and Geers, M., “FE2 computational homogenization for the thermo-mechanical analysis of heterogeneous solids,” *Computer Methods in Applied Mechanics and Engineering*, Vol. 198, No. 3, 2008, pp. 602–613. doi:10.1016/j.cma.2008.09.008.
- [9] Nguyen, V. P., Lloberas-Valls, O., Stroeve, M., and Sluys, L. J., “Homogenization-based multiscale crack modelling: From micro-diffusive damage to macro-cracks,” *Computer Methods in Applied Mechanics and Engineering*, Vol. 200, 2011, pp. 1220–1236. doi:10.1016/j.cma.2010.10.013.
- [10] Tikarrouchine, E., Chatzigeorgiou, G., Praud, F., Piotrowski, B., Chemisky, Y., and Meraghni, F., “Three-dimensional FE2 method for the simulation of non-linear, rate-dependent response of composite structures,” *Composite Structures*, Vol. 193, 2018, pp. 165–179. doi:10.1016/j.compstruct.2018.03.072.
- [11] Fritzen, F., Hodapp, M., and Leuschner, M., “GPU accelerated computational homogenization based on a variational approach in a reduced basis framework,” *Computer Methods in Applied Mechanics and Engineering*, Vol. 278, 2014, pp. 186 – 217. doi:<https://doi.org/10.1016/j.cma.2014.05.006>.
- [12] Aboudi, J., “A continuum theory for fiber-reinforced elastic-viscoplastic composites,” *International Journal of Engineering Science*, Vol. 20, No. 5, 1982, pp. 605–621. doi:10.1016/0020-7225(82)90115-X.

- [13] Haj-Ali, R., and Aboudi, J., “Nonlinear micromechanical formulation of the high fidelity generalized method of cells,” *International Journal of Solids and Structures*, Vol. 46, No. 13, 2009, pp. 2577–2592. doi:10.1016/j.ijsolstr.2009.02.004, URL <http://dx.doi.org/10.1016/j.ijsolstr.2009.02.004>.
- [14] Lagoudas, D. C., Gavazzi, A. C., and Nigam, H., “Elastoplastic behavior of metal matrix composites based on incremental plasticity and the Mori-Tanaka averaging scheme,” *Computational Mechanics*, Vol. 8, No. 3, 1991, pp. 193–203. doi:10.1007/BF00372689, URL <https://doi.org/10.1007/BF00372689>.
- [15] Bednarczyk, B. A., Aboudi, J., and Arnold, S. M., “Micromechanics modeling of composites subjected to multiaxial progressive damage in the constituents,” *AIAA Journal*, Vol. 48, No. 7, 2010, pp. 1367–1378. doi:10.2514/1.45671.
- [16] Naghipour, P., Arnold, S. M., Pineda, E. J., Stier, B., Hansen, L., Bednarczyk, B. A., and Waas, A. M., “Multiscale static analysis of notched and unnotched laminates using the generalized method of cells,” *Journal of Composite Materials*, Vol. 51, No. 10, 2017, pp. 1433–1454. doi:10.1177/0021998316651708.
- [17] Zhang, D., Patel, D. K., and Waas, A. M., “A novel two-scale progressive failure analysis method for laminated fiber-reinforced composites,” *Proceedings of the 56th AIAA/ASCE/AHS/ASC Structures, Structural Dynamics, and Materials Conference*, 2015. doi:10.2514/6.2015-0969.
- [18] Zhang, D., Waas, A. M., and Yen, C., “Progressive damage and failure response of hybrid 3D textile composites subjected to flexural loading, part II: Mechanics based multiscale computational modeling of progressive damage and failure,” *International Journal of Solids and Structures*, Vol. 75-76, 2015, pp. 321 – 335. doi:<https://doi.org/10.1016/j.ijsolstr.2015.06.033>, URL <http://www.sciencedirect.com/science/article/pii/S0020768315003480>.
- [19] Patel, D., and Waas, A., “Damage and failure modelling of hybrid three-dimensional textile composites: a mesh objective multi-scale approach,” *Philosophical Transactions of The Royal Society A-Mathematical Physical And Engineering Sciences*, Vol. 374, No. 2071, 2017. doi:10.1098/rsta.2016.0036.
- [20] Ladevèze, P., Passieux, J.-C., and Néron, D., “The LATIN multiscale computational method and the Proper Generalized Decomposition,” *Computer Methods in Applied Mechanics and Engineering*, Vol. 199, No. 21, 2010, pp. 1287 – 1296. doi:<https://doi.org/10.1016/j.cma.2009.06.023>, URL <http://www.sciencedirect.com/science/article/pii/S0045782509002643>.
- [21] Ricks, T. M., Lacy, T. E., Pineda, E. J., Bednarczyk, B. A., and Arnold, S. M., “Computationally efficient High-Fidelity Generalized Method of Cells micromechanics via order-reduction techniques,” *Composite Structures*, Vol. 156, 2016, pp. 2–9. doi:10.1016/j.compstruct.2016.05.093, URL <http://dx.doi.org/10.1016/j.compstruct.2016.05.093>.
- [22] Carrera, E., Cinefra, M., Zappino, E., and Petrolo, M., *Finite Element Analysis of Structures Through Unified Formulation*, John Wiley & Son Ltd, 2014. doi:10.1002/9781118536643.
- [23] Zappino, E., and Carrera, E., “Multidimensional Model for the Stress Analysis of Reinforced Shell Structures,” *Computer Methods in Applied Mechanics and Engineering*, Vol. 56, No. 4, 2018, pp. 1647 – 1661. doi:<https://doi.org/10.2514/1.J056384>.

- [24] Kaleel, I., Petrolo, M., Waas, A., and Carrera, E., “Micromechanical progressive failure analysis of fiber-reinforced composite using refined beam models,” *Journal of Applied Mechanics*, Vol. 85, No. 2, 2018, pp. 021004–021004–8. doi:10.1115/1.4038610.
- [25] Carrera, E., and Filippi, M., “A refined one-dimensional rotordynamics model with three-dimensional capabilities,” *Journal of Sound and Vibration*, Vol. 366, 2016, pp. 343 – 356. doi:<https://doi.org/10.1016/j.jsv.2015.12.036>, URL <http://www.sciencedirect.com/science/article/pii/S0022460X15010238>.
- [26] Cinefra, M., Petrolo, M., Li, G., and Carrera, E., “Variable kinematic shell elements for composite laminates accounting for hygrothermal effects,” *Journal of Thermal Stresses*, Vol. 40, No. 12, 2017, pp. 1523–1544. doi:10.1080/01495739.2017.1360165.
- [27] Varello, A., Pagani, A., Guarnera, D., and Carrera, E., “Analysis of Stokes flows by Carrera Unified Formulation,” *Advances in Aircraft and Spacecraft Science*, Vol. 5, No. 3, 2018, pp. 363–383. doi:10.12989/aas.2018.5.3.363.
- [28] Kaleel, I., Petrolo, M., Waas, A., and Carrera, E., “Computationally efficient, high-fidelity micromechanics framework using refined 1D models,” *Composite Structures*, Vol. 181, 2017, pp. 358–367. doi:<https://doi.org/10.1016/j.compstruct.2017.08.040>, URL <http://www.sciencedirect.com/science/article/pii/S0263822317324947>.
- [29] Reddy, J., *Mechanics of laminated composite plates and shells. Theory and Analysis*, 2<sup>nd</sup> ed., CRC Press, 2004.
- [30] Chiang, K., and Fulton, R., “Concepts and implementation of parallel finite element analysis,” *Computers & Structures*, Vol. 36, No. 6, 1990, pp. 1039 – 1046. doi:[https://doi.org/10.1016/0045-7949\(90\)90211-J](https://doi.org/10.1016/0045-7949(90)90211-J), URL <http://www.sciencedirect.com/science/article/pii/004579499090211J>.
- [31] Dagum, L., and Menon, R., “OpenMP: An Industry-Standard API for Shared-Memory Programming,” *IEEE Comput. Sci. Eng.*, Vol. 5, No. 1, 1998, pp. 46–55. doi:10.1109/99.660313, URL <https://doi.org/10.1109/99.660313>.
- [32] Clay, S., and Knoth, P., “Experimental results of quasi-static testing for calibration and validation of composite progressive damage analysis methods,” *Journal of Composite Materials*, Vol. 51, No. 10, 2017, pp. 1333–1353. doi:10.1177/0021998316658539.
- [33] Engelstad, S., and Clay, S., “Comparison of composite damage growth tools for static behavior of notched composite laminates,” *Journal of Composite Materials*, Vol. 51, No. 10, 2017, pp. 1493–1524. doi:10.1177/0021998316675945.
- [34] Zhang, D., Patel, D. K., and Waas, A. M., “A novel two-scale progressive failure analysis method for laminated fiber-reinforced composites,” *56th AIAA/ASCE/AHS/ASC Structures, Structural Dynamics, and Materials Conference*, 2015. doi:10.2514/6.2015-0969.
- [35] Catapano, A., and Montemurro, M., “A multi-scale approach for the optimum design of sandwich plates with honeycomb core . Part I : homogenisation of core properties,” *Composite Structures*, Vol. 118, 2014, pp. 664–676. doi:10.1016/j.compstruct.2014.07.057, URL <http://dx.doi.org/10.1016/j.compstruct.2014.07.057>.
- [36] Zhao, B., and Yu, W., “Multiscale Structural analysis of honeycomb structure using mechanics of structure genome,” *Proceedings of the American Society for Composites Thirty-second Technical Conference*, 2017, pp. 92–106. doi:10.12783/asc2017/15171.

- [37] Burton, W., and Noor, A., "Assessment of continuum models for sandwich panel honeycomb cores," *Computer Methods in Applied Mechanics and Engineering*, Vol. 145, No. 3, 1997, pp. 341 – 360. doi:10.1016/S0045-7825(96)01196-6, URL <http://www.sciencedirect.com/science/article/pii/S0045782596011966>.
- [38] Grediac, M., "A finite element study of the transverse shear in honeycomb cores," *International Journal of Solids and Structures*, Vol. 30, No. 13, 1993, pp. 1777 – 1788. doi:10.1016/0020-7683(93)90233-W, URL <http://www.sciencedirect.com/science/article/pii/002076839390233W>.